High Thermoelectric Performance of Multiwalled Carbon Nanotubes based Ionogels

Imran Haider Sajid[1,2*], Navid Aslfattahi[3], Mohd Faiz Mohd Salleh[4], Nik Nazri Nik Ghazali[1], R. Saidur[5, 6], Muhammad Tahir[7], Mohamed Bashir Ali Bashir[8,9], Mohd Faizul Mohd Sabri[1,10*].

[1]Department of Mechanical Engineering, Faculty of Engineering, Universiti Malaya, 50603 Kuala Lumpur, Malaysia.

[2]Physics Characterization and Simulations Lab (PCSL), Department of Physics, School of Natural Sciences (SNS), National University of Sciences and Technology (NUST), Islamabad, 44000, Pakistan

[3]Department of fluid Mechanics and Thermodynamics, Faculty of Mechanical Engineering, Czech Technical University in Prague, Tecchnika 4, 16000, Prague, Czech Republic.

[4]Department of Electrical Engineering, Faculty of Engineering, Universiti Malaya, 50603 Kuala Lumpur, Malaysia

[5]Research Centre for Nano-Materials and Energy Technology (RCNMET), School of Science and Technology, Sunway University, Bandar Sunway, Petaling Jaya, 47500, Selangor Darul Ehsan, Malaysia.

[6]Department of Engineering, Lancaster University, LA1 4YW, United Kingdom

[7]Department of Physics, Faculty of Physical and Numerical Sciences, Abdul Wali Khan University, Mardan, 23200, Pakistan.

[8]Department of Mechanical Engineering, College of Engineering, Jouf University, 42421, Sakaka, Saudi Arabia.

[9]Department of Mechanical Engineering, Faculty of Engineering, Eldaein University, 63312, Eldaein, Sudan.

[10] Centre for Energy Sciences, Universiti Malaya, 50603 Kuala Lumpur, Malaysia.

*Correspondence should be addressed to Mohd Faizul Mohd Sabri (email: faizul@um.edu.my) Imran Haider Sajid (ihsajid@gmail.com).

Abstract

Ionogels have emerged as promising thermoelectric materials with Seebeck coefficient 2-3 orders of magnitude higher than Seebeck coefficient of their inorganic counter parts. However, they suffer from the problem of low ionic conductivity, which can be improved with the addition of inorganic nanofillers to the ionogels. In the present work, thermoelectric performance of multiwall carbon nanotubes based ionogels (IGs) has been investigated. IGs were synthesized via in situ radical polymerization of polyethylene glycol 200 dimethacrylate

(PEG200DMA) difunctional monomer in the presence of 1-butyl-3-methyl imidazolium tetrafluoroborate (an ionic liquid) and MWCNTs. Three composites namely MWCNTs-0.25, MWCNTs-0.5 and MWCNTs-1 were prepared having the concentration of MWCNTs by 0.25, 0.5 and 1 wt. % respectively. A remarkable 75.3% enhancement in ionic conductivity was achieved for the MWCNTs-1 wt. % ionogel compared to the base IG at 40 °C. This substantial improvement can be attributed to the "breathing polymer chain model," which describes the dissociation of ion aggregates due to the interaction between the ionic liquid and polymer chains. In terms of thermoelectric performance amongst the MWCNT ionogels, 0.25 wt. % MWCNT-based ionogels was the optimized concentration with very high Seebeck coefficient of 1.70 mV/K and power factor of 4.1 μW/m. K along with excellent thermal stability up to 386 °C. These high-performing ionogels hold great promise for efficient utilization of low-grade thermal energy.

Keywords: ionic Seebeck coefficient, ionic conductivity, thermal conductivity, multiwall carbon nanotubes, ionogel.

1. Introduction

The utilization of thermal energy from sources such as sunlight, fossil fuels, geothermal energy, and mechanical work is crucial for various applications. However, a significant portion of this energy is wasted in the form of heat released into the environment. For instance, it has been reported that nearly 50% of the total energy required in the United States is lost as heat from factories operating below 130 °C [1]. This waste heat can be harnessed and converted into electricity, thus contributing to addressing the global energy shortage [2].

Solid-state thermoelectric generators (TEGs) offer a promising solution for converting low-grade waste heat into useful electrical energy. They outperform liquid-state thermo-electrochemical cells, which often face challenges such as leakage [3, 4]. By developing

environmentally friendly and cost-effective thermoelectric modules, significant strides can be made towards sustainable green energy solutions [5, 6].

The thermoelectric figure of merit (ZT), a dimensionless parameter, provides valuable insights into the thermoelectric performance of materials. It can be calculated using Equation (1):

$$ZT = (S^2.\sigma.T)/K \quad (1)$$

Here, S, σ, K, and T represent the Seebeck coefficient, electrical conductivity, thermal conductivity, and temperature, respectively [7-10]. According to Eq. (1), ZT is directly related to the square of Seebeck coefficient which is another important parameter for thermoelectric materials and small changes in S may have profound effect on value of ZT. The Seebeck coefficient and electrical conductivity of thermoelectric polymers are also interdependent and are inversely related, analogous to inorganic semiconductors [11]. Thermoelectric materials can be classified into two categories based on their conduction mechanism: electronic conductors and ionic conductors. The majority of thermoelectric materials fall under the electronic conductor category, comprising inorganic conductors and semiconductors. However, these electronic-based thermoelectric devices, consisting of p-type and n-type materials connected in series, often exhibit low Seebeck coefficients of the order of μV/K, limiting their efficiencies [12-14].

The low Seebeck coefficient in electronic thermoelectric materials arises from the symmetric distribution of the density of states around the Fermi level (EF). This results in an almost equal number of hot and cold electrons above and below the EF, respectively. Consequently, the electrons diffusing from the hot side to the cold side are roughly equal to those moving in the opposite direction due to the temperature gradient [15]. Notable efforts have been made to enhance the Seebeck coefficient in electronic TE materials. For example, Bi_2Te_3-ySey electrodeposited thin films achieved a Seebeck coefficient of 120 μV/K [16], and

nanowires of P-type Bi-Sb-Te exhibited a Seebeck coefficient of 138 μV/K [17]. Furthermore, Ag_2Se-based n-type materials demonstrated a thermoelectric figure of merit of 1.2 at room temperature, with a Seebeck coefficient of approximately -200 μV/K [18].

To achieve practical thermovoltage for applications, electronic TE materials require a large number of TE legs connected in series due to their low Seebeck coefficients. This complexity increases the design and cost of TE modules. In contrast, ionic conductors have received less attention for thermoelectric conversion compared to electronic conductors. Ionic thermoelectric conductors can exhibit Seebeck coefficients several orders of magnitude higher than their electronic counterparts. The Seebeck coefficient in ionic TE materials is attributed to the conduction of ions, and it can be expressed using Equation (2):

$$S_i = V_{thermal} / \Delta T \quad (2)$$

Here, S_i represents the Seebeck coefficient for ionic thermoelectric materials, and $V_{thermal}$ denotes the potential difference generated due to the temperature gradient (ΔT) [19]. Ionic thermoelectric conductors, such as thermoelectrochemical cells (TECs) or thermo-cells, have demonstrated promising performance in low-grade heat harvesting, with Seebeck coefficients in the range of mV/K.

TECs employ redox couples, ionic liquids, or molecular solvents to convert waste heat into electricity. Ionic liquids, with their high ionic conductivity, low thermal conductivity, low vapor pressure, and high thermal stability, offer attractive properties for this purpose. For instance, TECs utilizing a mixture of iodide/triiodide (I^-/I_3^-) redox couple and 1-butyl-3-methylimidazolium tetrafluoroborate [bmim][BF_4] as an electrolyte achieved a Seebeck coefficient of 0.44 mV/K [7]. Migita et al. reported a Seebeck coefficient of -1.49 mV/K for the redox couple $[Fe(CN)6]^{3-/4-}$ in the ionic liquid [C_4mpyr][NTf_2] [20]. Aqueous thermogalvanic cells also exhibited a large Seebeck coefficient of 4.2 mV/K [21]. However, the liquid nature of TECs limits their practical application in device fabrication.

To overcome the challenges posed by liquid TECs, an innovative approach involves confining ionic liquid electrolytes within a polymer matrix to form a 3-dimensional solid structure while preserving the key property of ionic conductivity. This emerging class of materials, known as ionogels (IGs), immobilizes ionic liquids within a polymer matrix [22, 23]. IGs have shown high Seebeck coefficients but relatively low ionic conductivity compared to electronic TE materials. The addition of inorganic nanofillers to ionogels can enhance their ionic conductivity. Researchers have explored the concept of creating nanocomposites by incorporating inorganic nanofillers into conducting polymers [24, 25]. For instance, the thermoelectric performance of PVDF and MWCNTs nanocomposites has been investigated [26]. Polyaniline and bismuth nanocomposites have demonstrated high Seebeck coefficients, benefiting from the synergistic effect between the constituents [27]. Carbon nanotubes (CNTs) are particularly promising for incorporation into ionogels due to their high electrical conductivity and low thermal conductivity when combined with polymers [28-31]. The addition of CNTs into an Ag_2Te matrix led to an enhanced thermoelectric power factor through improved electrical conductivity [32, 33]. Notably, there is a lack of literature on the utilization of multiwalled carbon nanotubes (MWCNTs) to enhance the thermoelectric performance of ionogels.

This study presents the incorporation of 1-butyl-3-methyl imidazolium tetrafluoroborate and multiwall carbon nanotubes (MWCNTs) into the PEG200DMA polymer matrix, aiming to develop ionogels with enhanced thermoelectric performance. The objectives of this paper encompass the synthesis and characterization of $BMIMBF_4$/MWCNTs/PEG200DMA composite ionogels, the evaluation of the impact of three distinct weight % concentrations (0.25, 0.5, and 1 wt. %) of MWCNTs on the thermoelectric performance of ionogels, the investigation of the thermal and structural properties of the synthesized ionogels, and the determination of the optimized weight % of MWCNTs to achieve desirable thermoelectric

performance. By addressing these objectives, this study aims to contribute to the development of efficient and cost-effective thermoelectric materials for sustainable energy applications.

2. Experimental Details

2.1 Materials

The multiwall carbon nanotubes were obtained from US Research Nanomaterials, Inc., located in Houston, Texas, USA. Polyethylene glycol 200 dimethacrylate and 1-butyl-3-methyl imidazolium tetrafluoroborate ([BMIM]BF_4) were procured from Geo Specialty Chemicals (USA) and Merck (Germany), respectively. The grade 316 stainless steel coin cells (CR2032) used in the study were provided by GELON Lib Co., Ltd. from China.

2.2 Preparation of Ionogels

The preparation of ionogels involved the polymerization of PEG200DMA difunctional monomer, using azobisisobutyronitrile (AIBN) as free radical initiator. Firstly, the ionic liquid (60 wt. %) and PEG200DMA (40 wt. %) were mixed at room temperature with stirring at 500 rpm. Then AIBN was then added by 1 wt. % into above mixture and stirred at 500 rpm for 10 minutes at 60 °C. Once AIBN was homogeneously mixed with the combination of PEG200DMA and BMIMBF4, the polymerization was performed at 90 °C, resulting in the formation of a 3D solid polymer matrix that immobilized the IL, referred to as ionogel [34].

For the preparation of MWCNTs ionogels, the entire process was repeated with the additional step of heating the precursor of MWCNTs, BMIMBF4, and PEG200DMA for four hours at 60 °C to achieve uniform mixing of MWCNTs. As a result of heat treatment at 90 °C, AIBN became free radical, which attach on the olefinic bond in the PEGDMA resulting in a new free radical on one of the carbons involved in olefinic bond. This free radical on carbon continue to attack the neighbouring molecules and chain growth continues. When the concentration of the repeating units decreases to very low value the termination takes place by the combination of the growing ends of the chains. Figure S1 illustrates the synthesized base ionogel and the MWCNTs ionogel. The MWCNTs content was varied at 0.25, 0.5, and 1 wt.%

to prepare the MWCNTs ionogels, denoted as MWCNTs-0.25, MWCNTs-0.5, and MWCNTs-1, respectively. Figure 1 presents a schematic diagram depicting the synthesis of MWCNT ionogels.

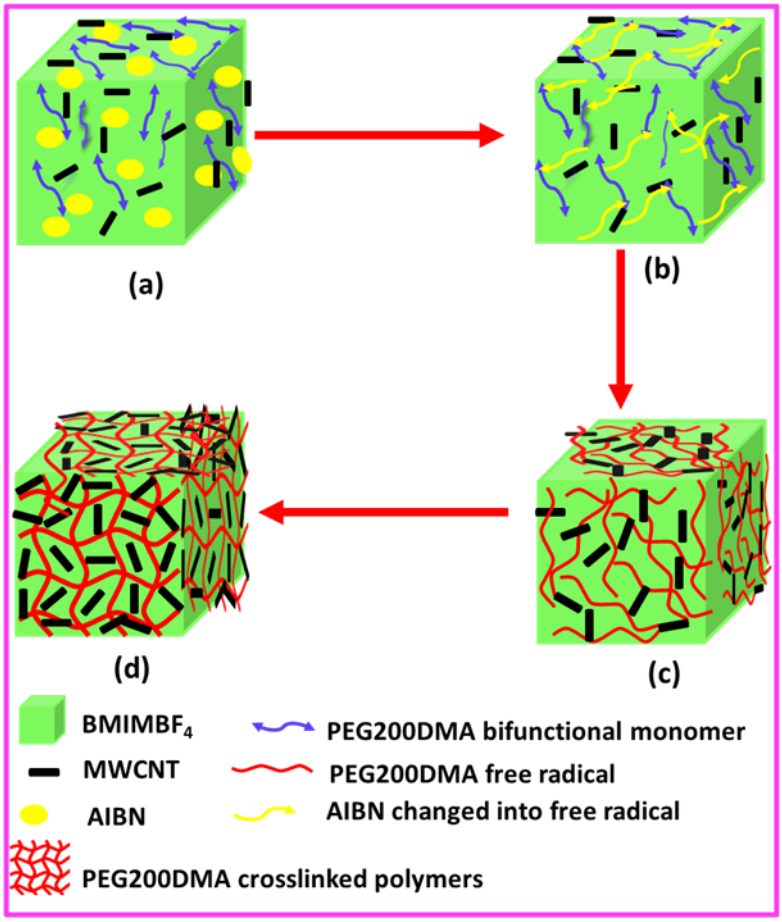

Fig. 1. Scheme for the synthesis of MWCNT ionogels (a) Mixture of BMIMBF4, PEG200DMA and AIBN (b) when the precursor is heated at 90 °C, AIBN decomposes and changes into free radical and attacks the PEG200DMA difunctional monomer (c) The PEG200DMA monomer becomes a free radical after reaction with the AIBN radical (primary radical) or after attachment to the active centre of the growing polymer chain. (d) all PEG200DMA radicals are covalently bonded with each other to form crosslinked PEG200DMA polymers.

2.3 Characterizations of Ionogels

2.3.1 Measurement of Ionic Conductivity

The ionic conductivity of the ionogels was determined by sandwiching them between two stainless steel electrodes of LIR2032 coin cells. The thickness of the ionogels (IGs) was measured to be 0.2 cm using a digital Vernier Caliper and its surface area was 1.76 cm^2. The impedance of the ionogels was measured using electrochemical impedance spectroscopy, employing a Gamry reference 600. The measurements were conducted over a frequency range from 1 Hz to 100 kHz.

To investigate the temperature dependence of impedance, the measurements were performed in a temperature range of 40 °C to 70 °C. Before each measurement, the samples were allowed to thermally equilibrate for 15 minutes after reaching the desired temperature. A schematic diagram illustrating the experimental setup for the measurement of ionic conductivity is presented in supplementary Figure S_2.

2.3.2 Measurement of Seebeck Coefficient

To measure the Seebeck coefficient of the ionogels, a temperature gradient is created by placing a ceramic heater and Peltier cooler across two electrodes of the coin cell. The temperature of the heater is manually increased using a DC power supply (KEITHLEY 2231A-30-03) to generate the desired thermal gradient. Two thermocouples are used to measure the temperature of the hot and cold sides. The voltage generated by the temperature gradient is measured using a digital multimeter (Agilent 34461A61/2).

Before starting the measurement, the temperature gradient is carefully maintained with a temperature fluctuation of ± 0.5 °C. To ensure thermal equilibrium, a waiting period of 10 minutes is included after each step increase in the power supply voltage. Five values of open-

circuit voltage are recorded within a two-minute interval. The Seebeck coefficient is determined by calculating the slope of the graph depicting the relationship between the temperature gradient and the potential difference. The experimental setup used for measuring the Seebeck coefficient is described in our previous work by Sajid et al. [35].

2.3.3 Measurement of Thermal conductivity

The thermal conductivities of the ionogels were determined using a Linseis THB500 instrument. The thermal conductivity measurement range of THB 500 is from 0.01 up to 500 W/ (m.K) with an accuracy better than 5%. The measurements were conducted with a measuring current of 5mA and a power of 15 mW, and each measurement had a duration of 8 seconds. The thermal conductivity measurement employed the Quasi-Steady-State (QSS) technology. The instrument utilized a Hotpoint sensor, which is capable of measuring thermal conductivity for small sample sizes. The small size of the Hotpoint sensor (4.5 mm) minimizes any potential side effects during the measurement process, ensuring accurate results.

2.3.4 Thermogravimetric analysis

Thermogravimetric analysis (TGA) of the MWCNTs ionogels was performed using a Perkin Elmer TGA 4000 instrument. The samples were placed in alumina crucibles with a volume of 180 µL, known for their high temperature resistance up to 1750 °C. The analysis was conducted under a nitrogen atmosphere with a flow rate of 19.8 ml per minute. The heating rate used was 10 °C per minute, starting from an initial temperature of 30 °C and ramping up to 500 °C using a sample mass of 8.6 mg. The acquired data from the TGA experiments were analyzed using Pyris Software, a specialized software for thermogravimetric analysis.

2.3.5 Fourier Transform Infrared Spectroscopy

The Perkin Elmer Spectrum-II FTIR spectrometer with a $LiTaO_3$ (lithium tantalate) MIR detector was used to run the FTIR spectroscopy of ionogels from wavenumber of 350 to 4000 cm^{-1} performing 16 scans and resolution equal to 4 cm^{-1}. The baseline and ATR corrections were applied to the FTIR results.

2.3.6 XRD Analysis

X-ray diffraction of the ionogels was performed using powder X-ray diffraction (Rigaku, Miniflex). The characteristics Cu Kα radiation with a wavelength of λ=1.5406 Å and voltage of 40 kV along with 15mA of current were used to perform XRD. The range of the angle was from 3 to 90° and a scan rate of 10° /min was utilized during the XRD analysis.

2.3.7 Microstructural Characterization

A scanning electron microscope (SEM) from TESCAN VEGA3 was used to study the morphology of ionogels. Before SEM operation, the samples were coated with platinum using the Quorum (Q150R S) rotary pumped coater with 30 mA of sputtering current. To perform the FETEM, the ionogels were mixed with ethanol followed by heating for five hours at 90 °C to mix homogeneously. After that, the diluted samples were shifted to copper grids and allowed to dry in air for 24 hours.

3 Results and Discussion

3.1 Fourier transforms infrared Spectroscopy of ionogels

The interactions between the ionic liquid (IL), MWCNTs, and poly (PEG200DMA) matrix were analyzed using FTIR spectroscopy, and the corresponding results are presented in Figure

2. In the spectrum of the base ionogel, peaks were observed at 3161 cm^{-1} and 3181 cm^{-1}, which can be attributed to the symmetric (C-H) stretch of the imidazolium cation. The peaks corresponding to the B-F stretch in the BF_4 anion of the IL were found at wavenumbers of 521 cm^{-1} and 1049 cm^{-1} [36]. The peaks associated with the butyl chain of [BMIM]BF4 were observed in the range of 2800-3000 cm^{-1}. At a wavenumber of 1169 cm^{-1}, a peak was observed related to the C=N stretching vibration. The C=O (carbonyl group) peak of methyl acrylate in poly (PEG200DMA) was positioned at 1724 cm^{-1}. Peaks at 941 cm^{-1} and 1636 cm^{-1} were attributed to the C=C stretch of the methacrylate group attached to polyethylene glycol as observed by Jiao et al [37]. The presence of the ester group (C-O) was indicated by a band observed at 1188 cm^{-1} [38, 39]. In the FTIR spectrum, a shift of the peak at 1048 cm^{-1} in the base gel was observed to 1038 cm^{-1} in the spectrum of MWCNTs-0.5. Additionally, the transmission of infrared radiation decreased from 32.4% to 23.79%, suggesting the formation of new bonds, possibly due to interactions between MWCNTs, poly (PEG200DMA), and $[BMIM]BF_4$. It is speculated that the imidazolium cations may be covalently linked with the MWCNTs [40].

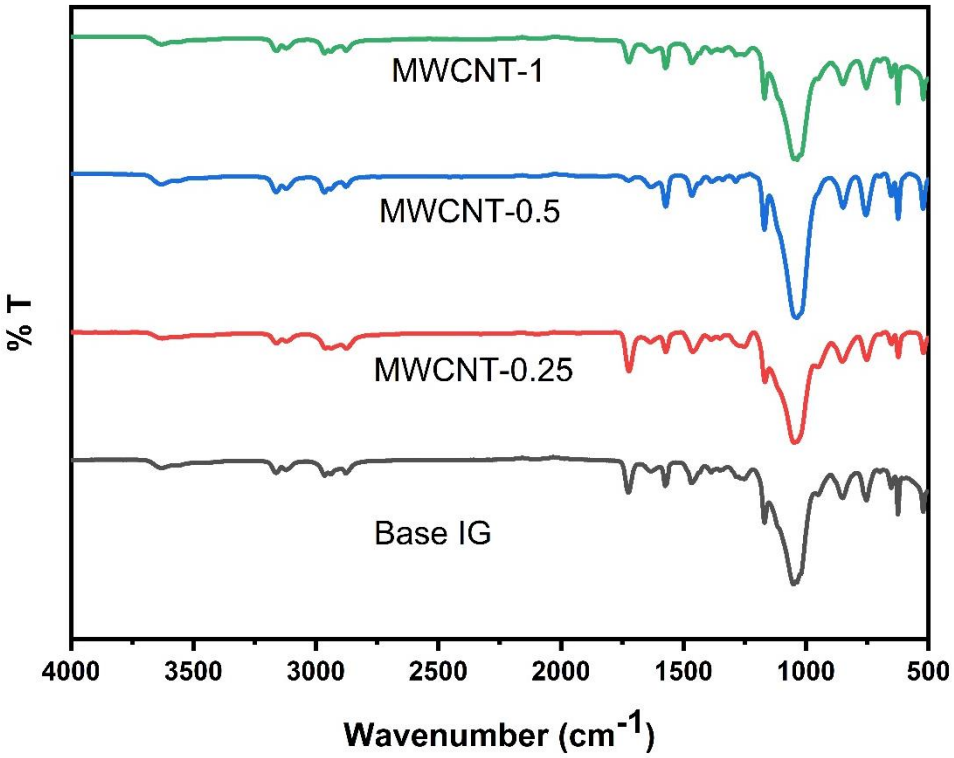

Fig. 2. FTIR Spectra of base gel and MWCNTs ionogels have been stacked for comparison.

3.2 XRD Analysis of Ionogels

The XRD graphs of the ionogels revealed their amorphous nature, as indicated by the presence of broad peaks, as shown in Figure 3. In the XRD pattern of the base ionogel, a broad hump with the highest intensity was observed at 2θ equal to 22.5° indexed as (002) plane and is attributed to PEGDMA which is a characteristics of amorphous polymer[41]. The broadness of the peak indicates the ordering of main polyether chains due to interaction between them. Another peak at 9.5° which shows the presence of ionic liquid [BMIM]BF_4 [42, 43]. The XRD graph of pristine MWCNT indicates a sharp and strong peak at 2θ equal to 26° which can be indexed as (002) reflection of the graphite confirming the graphitic structure of the MWCNTs. Another peak at corresponds to (100) plane of MWCNTs [44]. After the incorporation of MWCNTs into ionogel, the 002 peak of the base ionogel has been slightly shifted to lower scattering angle equal to 20.9° from 22.5°. The reduction in peak intensity in MWCNTs-0.25,

compared to the base IG, suggests that the ionogel maintains its amorphous nature while MWCNTs are uniformly distributed within it. However, with a further increase in the amount of MWCNTs, the XRD patterns of MWCNTs-0.5 and MWCNTs-1 demonstrated an increase in peak intensity. This increased intensity can be attributed to the formation of MWCNT aggregates within these ionogels. Interestingly, an increasing trend in the amorphous nature of the ionogels was observed with an increase in the weight content of MWCNTs, ranging from 0.25 to 1 wt.%.

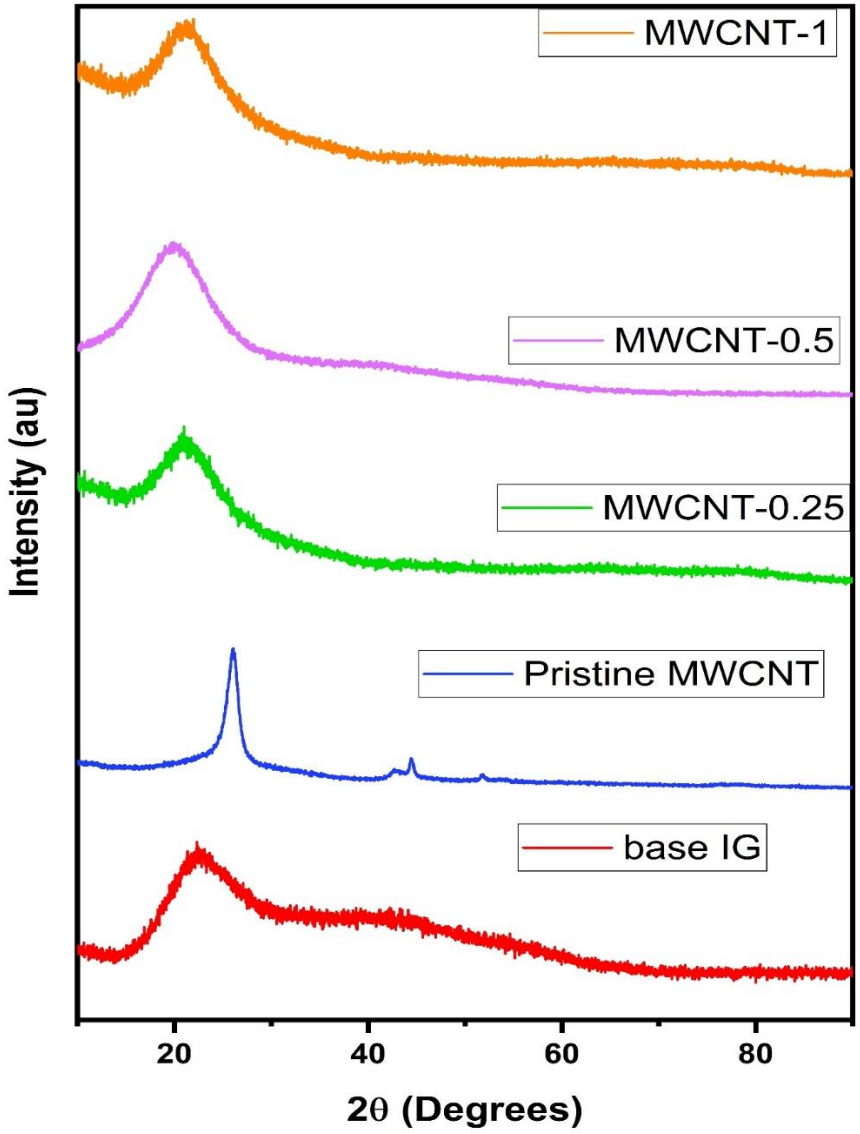

Fig. 3. XRD graphs of base ionogel, pristine MWCNT and MWCNTs ionogels. XRD analysis was performed with an angle ranging from 3 to 90° at a scan rate of 10° /min.

3.3 Thermogravimetric analysis of synthesized Ionogel/MWCNTs

The thermal stability of the base ionogel and MWCNT ionogels with different loading concentrations (0.25, 0.5, and 1 wt. %) was evaluated using thermogravimetric analysis (TGA) and is presented in Figure 4(a). The TGA measurements were conducted with a heating rate of 10 °C/min in the temperature range of 30-500 °C for all samples. It was observed that the initial and final degradation temperatures of the base ionogel increased with the inclusion of 0.25 and 1 wt. % loading concentrations of MWCNTs. This enhancement in thermal stability is consistent with previous research by Moganty et al. [45], who demonstrated improved thermal stability in an ionic liquid (IL) system with the inclusion of SiO_2 nanoparticles. However, the synthesized MWCNT ionogels with a loading concentration of 0.5 wt. % exhibited lower thermal stability compared to the base ionogel. The highest mass loss of the base gel shifted from 371 to 386 °C with the inclusion of 0.25 wt. % of MWCNTs.

In terms of the initial decomposition temperature (IDT), the synthesized ionogel-MWCNT with loading concentrations of 0.25 and 1 wt. % showed higher values compared to the base gel. In a separate research work by Fredlake et al. on the ionic liquid [BMIM]BF4, the IDT was reported at 315 °C [46]. This indicates that the immobilization of the ionic liquid in the polymer matrix has improved the thermal stability. However, the IDT of the ionogel-MWCNT with a loading concentration of 0.5 wt. % was similar to that of the base gel, with negligible changes. The values of IDT of all the samples have been shown in table 1 in supplementary files. The same trend was observed for the half decomposition temperature (D ½) and residual mass also called final residue (FR) of the ionogel-MWCNT with loading concentrations of 0.25

and 1 wt. %. Figure 4(c) shows the enhancement in the D ½ and FR regions for the synthesized ionogels with the inclusion of MWCNTs at loading concentrations of 0.25 and 1 wt. %.

The thermal stability of the ionogel improved due to the addition of MWCNTs in the base ionogel (IDT at 370 °C), as indicated by the higher value of IDT for MWCNTs-0.25 at 386 °C. The improvement in thermal stability can be attributed to the intricate interactions between the anion (BF_4^-) and the polymer matrix, as indicated by the shifting of the peak related to B-F stretch in the FTIR spectrum of MWCNT ionogels from a wavenumber of 1048 cm^{-1} to 1038 cm^{-1}. However, the thermal stability of the ionogel-MWCNT with a loading concentration of 0.5 wt. % in the FR region was reduced compared to the base gel. This could be attributed to the aggregation of MWCNTs within the ionogel matrix. Since MWCNTs have a high specific surface area (SSA), the interface interactions between MWCNTs and the base gel matrix at higher temperatures might increase the activation energy, which is directly related to the decomposition temperature [47]. This may explain the different behaviour of MWCNT ionogels with a loading concentration of 0.5 wt. % in terms of thermal stability. Zhou et al. investigated the effects of the filler size and content on thermal properties and thermal stability of polypropylene (PP) composite. He observed an obvious increase in thermal stability for the PP/TNIM2 and PP/TNIM3 systems with the MWCNT weight fraction when the MWCNT weight fraction is lower than 1 wt.%, and then increase slightly at the filler range from 1 to 4 wt.%, but decrease slightly at the filler content higher than 4 wt.%. For the PP/TNIM4 and PP/TNIM8 systems, the values of the starting decomposition temperature increase nonlinearly with the MWCNT weight fractions filled with four different sizes of multi-walled carbon nanotubes (MWCNTs) [48] .

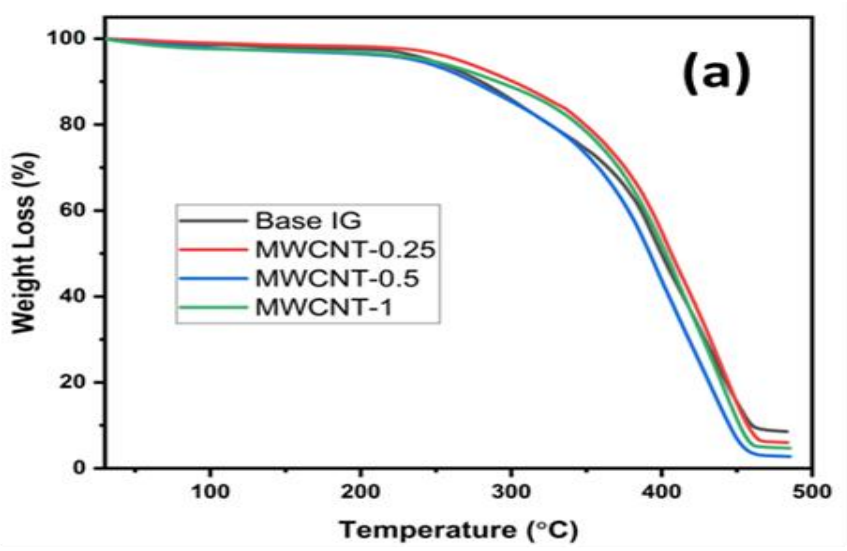
(a)
Weight Loss (%)
Temperature (°C)
Base IG
MWCNT-0.25
MWCNT-0.5
MWCNT-1

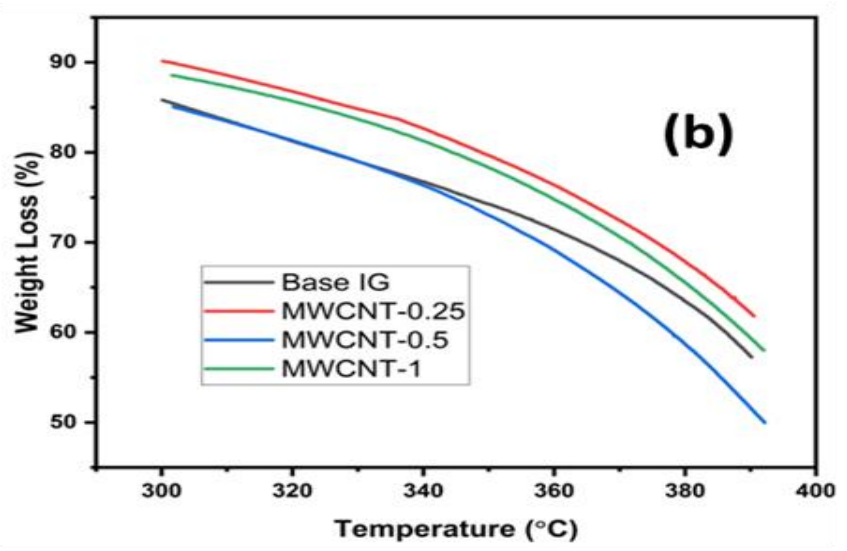
(b)
Weight Loss (%)
Temperature (°C)
Base IG
MWCNT-0.25
MWCNT-0.5
MWCNT-1

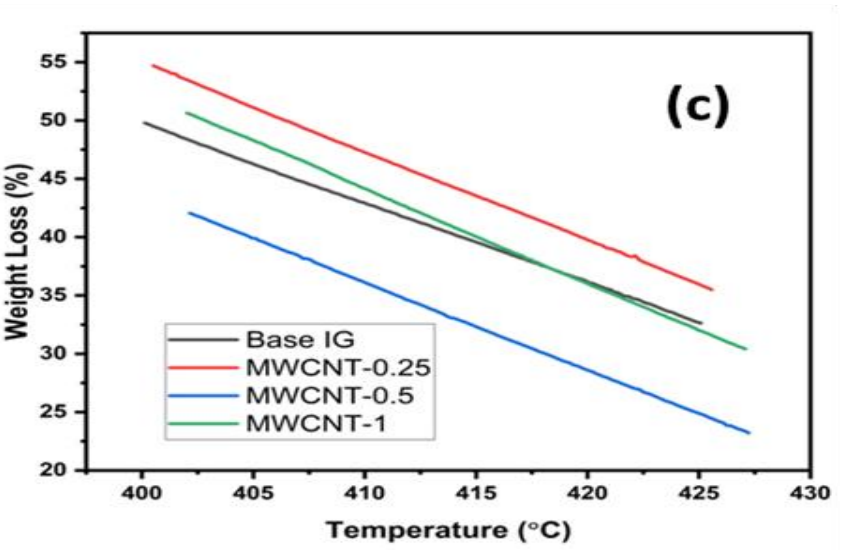
(c)
Weight Loss (%)
Temperature (°C)
Base IG
MWCNT-0.25
MWCNT-0.5
MWCNT-1

Fig. 4. (a) TGA thermograms of base ionogel and MWCNTS ionogels. Perkin Elmer TGA 4000 was employed to perform a thermogravimetric analysis of ionogels, (b) IDT of the synthesized ionogels, (c) FR of the synthesized ionogels.

3.4 Morphological Characterization of ionogels

The scanning electron microscopy (SEM) images of the ionogels are presented in Figure 5. The SEM images of the base ionogel revealed an interconnected network of ionic and polymer chains. With a varied chemical composition and electrically charged solvents, ionic liquids (ILs) can engage in numerous physical (non-covalent) interactions with polymer networks. Good compatibility may lead to the formation of electrostatic, dipole-dipole, ionic, and hydrogen bonds between polymer chains and ILs, exemplifying the diverse ways in which they can interact [49].However, upon the incorporation of MWCNTs into the ionogels, these networks transformed into overlapping sheets-like structures. This change in morphology may be attributed to the large aspect ratio of the MWCNTs. The elemental mapping of the ionogels, shown in supplementary Figure S_4, indicated the presence of Carbon, Boron, Nitrogen, and Fluorine in all regions of the ionogels. This suggests a homogeneous distribution of the ionic liquid ([BMIM]BF4) and MWCNTs within the polymer matrix. Furthermore, Figure S3 displays the FETEM (Field Emission Transmission Electron Microscopy) images of the MWCNTs-0.25 ionogels at four different resolutions. These images reveal the presence of conducting channels formed by the multiwall carbon nanotubes throughout the ploy (PEG200DMA) matrix. This observation highlights the conductive nature of the MWCNTs and their ability to form continuous pathways within the polymer matrix.

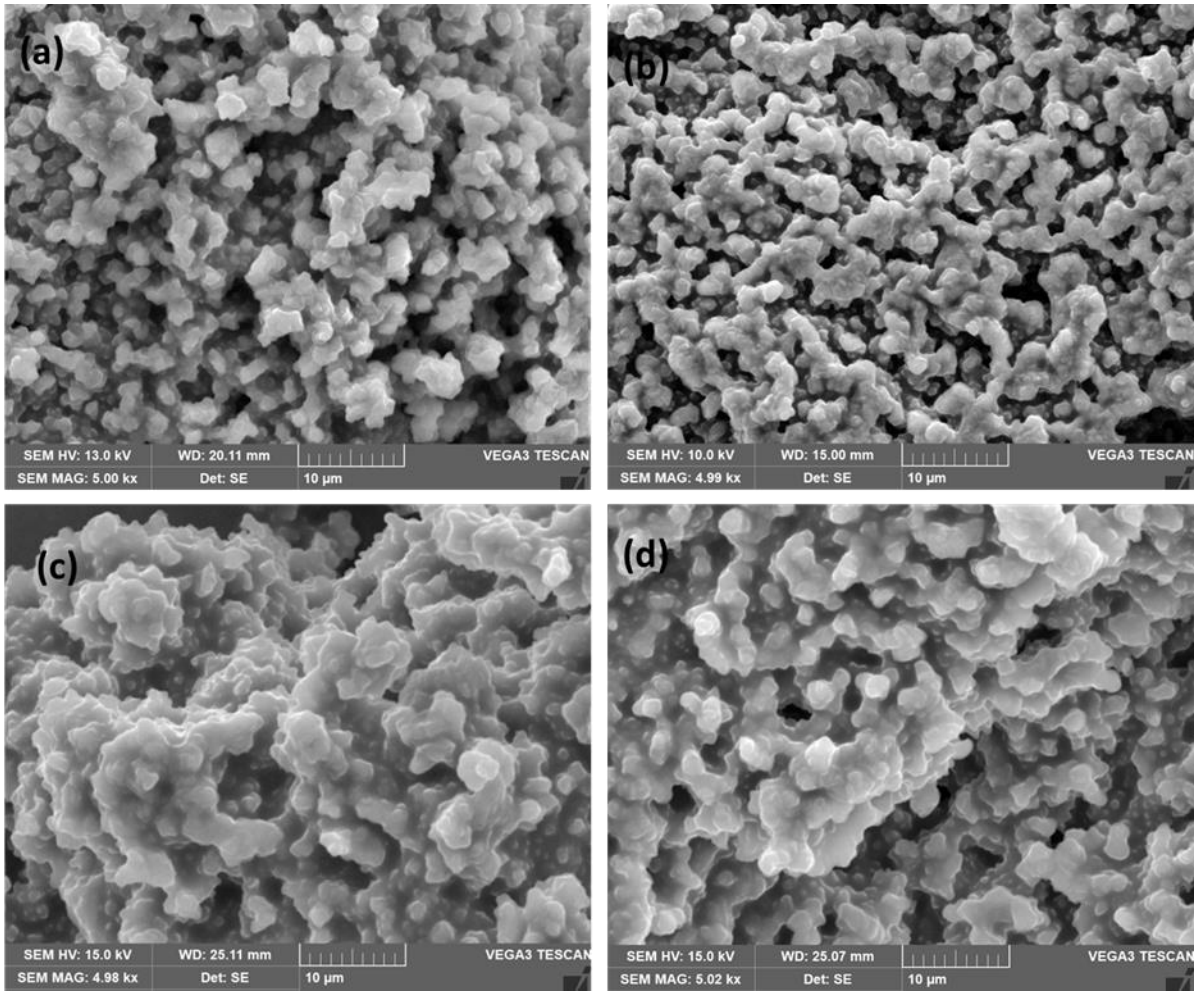

Fig. 5. SEM images of (a) base ionogel (b) MWCNT-0.25 IG (c) MWCNT-0.5 IG, and (d) MWCNT-1 IG. The ionogel samples were platinum coated by using the Quorum (Q150R S) rotary pumped coater with a sputtering current of 30 mA before scanning.

3.5 Ionic conductivity of Ionogels

The effect of varying MWCNTs concentration from 0.25 to 1 wt. % on the ionic conductivity of the ionogels has been investigated. The base ionogel exhibited an ionic conductivity of 7.3 mS/cm. However, upon the addition of 1 wt. % of MWCNTs to the base ionogel, a significant increase of 75% in the ionic conductivity was observed. As displayed in supplementary Fig. S5 “Nyquist” plot is used to portray the relation between real (Z′) and imaginary (Z″) parts of impedance. The x-axis intercept of the Nyquist plot shows the bulk resistance (R_b) of the ionogel. The Fig. S5 demonstrates that with increase in temperature the

R_b of the base ionogel decreased. The highest ionic conductivity of 15.8 mS/cm was achieved in the MWCNTs-1 ionogel. The calculation of ionic conductivity was performed using Equation 3:

$$\sigma = L / AR_b \quad (3)$$

Here, L represents the thickness of the ionogels in centimeters (cm), A represents the area of the ionogels in square centimeters (cm^2), and R_b represents the bulk resistance of the ionogels in ohms (Ω).

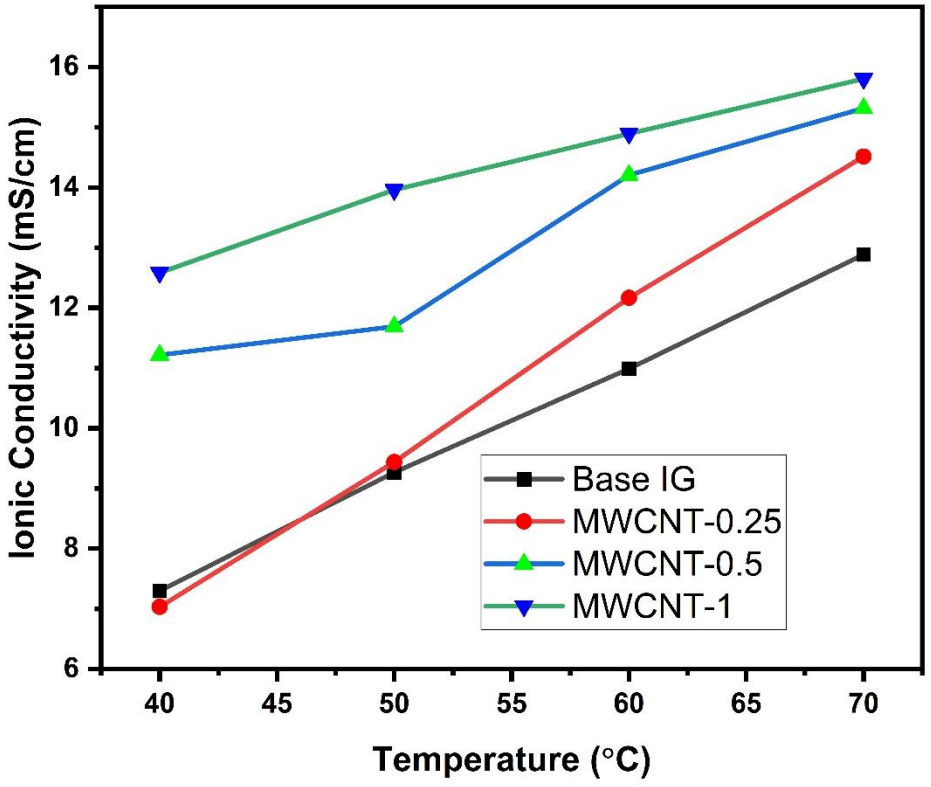

Fig. 6. The ionic conductivity of base ionogel and MWCNTs IGs is plotted versus temperature.

Figure 6 depicts the ionic conductivity of the ionogels in the temperature range of 40 to 70 °C. The results show a linear increase in the ionic conductivity of the ionogels with the rise in temperature, which is consistent with the behavior observed in semiconductors. This increase in ionic conductivity can be attributed to the breaking of ion aggregates within the ionic liquid,

resulting in a greater number of charge carriers available for conduction. Furthermore, the decoupling of cation and anion transport from the segmental motion of polymers also contributes to the enhancement of ionic conductivity, as reported by Susan et al.[50]. With increasing temperature, the viscosity of the ionic liquid decreases, facilitating the motion of ions. This phenomenon is explained by the "breathing polymeric chain model," which suggests that the dissociation of ion aggregates occurs as polymer chains fold and unfold [51, 52]. Overall, the rise in temperature promotes the mobility of ions and leads to an increase in the ionic conductivity of the ionogels.

3.6 Seebeck Coefficient of Ionogels

Figure 7 presents the Seebeck coefficient of the ionogels. The base ionogel exhibited a Seebeck coefficient of 1.93 mV/K. The inclusion of 0.25 wt.% MWCNTs resulted in a slightly reduced Seebeck coefficient of 1.70 mV/K. However, with further increases in the MWCNTs concentration to 0.5 and 1 wt.%, the Seebeck coefficient decreased to 0.76 and 0.50 mV/K, respectively. The decrease in the Seebeck coefficient with increasing MWCNTs concentration can be attributed to the inverse relationship between the Seebeck coefficient and electrical conductivity of thermoelectric materials. The Seebeck coefficient is dependent on the average transport energy of charge carriers, while electrical conductivity is determined by the number of charge carriers. Therefore, an increase in the carrier concentration leads to enhanced electrical conductivity but a decrease in the Seebeck coefficient [53]. The positive sign of the Seebeck coefficients indicates that the majority charge carriers in the ionogels are imidazolium cations, suggesting a p-type behavior. In most ionic thermoelectric materials p-type behaviour has been observed since cations are usually more mobile than anions in electrolytes [54]. Several authors like Liu et al. and Zhao et al. have reported the p-type behavior of ionogels[55, 56]. The FTIR results of the ionogels also suggest possible interactions between the BF_4^- anion

and polymer chains, which may restrict anion mobility and result in relatively more mobile cations.

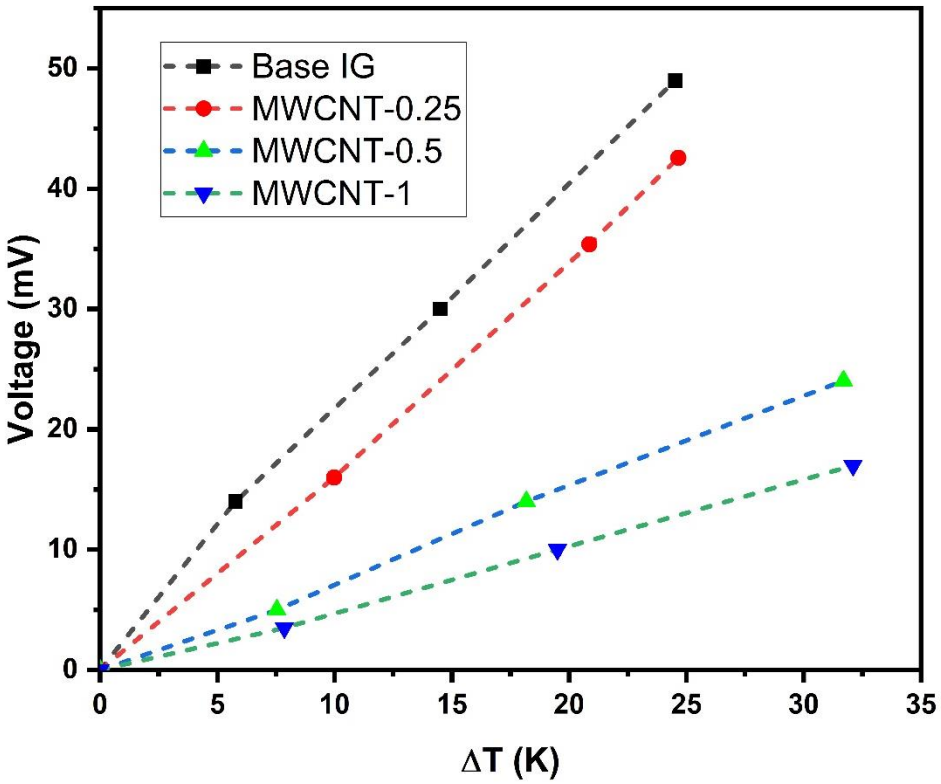

Fig. 7. The Seebeck coefficient of base ionogel and MWCNTs ionogels. The slope of the trend line is the value of the Seebeck coefficient.

3.7 Thermal Conductivity of Ionogels

Figure 8 illustrates the behavior of thermal conductivity of the ionogels with increasing temperature. At 33 °C, the thermal conductivity of the base ionogel was measured to be 0.110 W/m·K. Upon the addition of MWCNTs to the base ionogel, the thermal conductivity of MWCNTs ionogels initially increases for MWCNTs-0.25 and MWCNTs-1 then decreases for MWCNTs-0.5 ionogels. The highest thermal conductivity value of 0.165 W/m·K was observed at 63 °C. A similar trend in the thermal conductivity of flexible quasi solid-state ionogels has been reported by Cheng et al. [57].

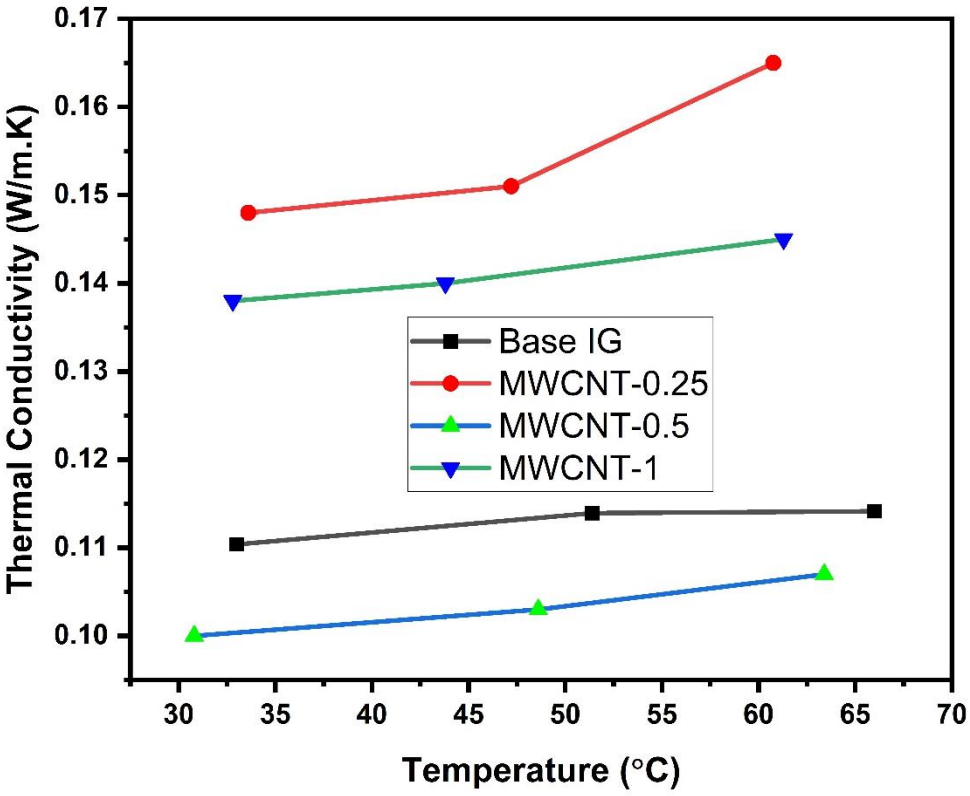

Fig. 8. Variation of thermal conductivity of base ionogel and MWCNTs ionogels with temperature.

The thermal conductivity of the ionogels depends on lattice vibrations, and it can be decreased when the lattice vibration between two phases is disrupted. The variation in thermal conductivity with MWCNTs loading can be attributed to the disruption of lattice vibrations between the polymer networks and MWCNTs. The literature on thermal conductivity of MWCNT composites has demonstrated a nonlinear dependence on the concentration of MWCNTs[58] . Upon incorporating 0.25 wt.% of MWCNTs into the base ionogel, an increase in thermal conductivity from 0.110 to 0.148 W/m·K is observed. This increase may be attributed to the uniform distribution of MWCNTs in the polymer matrix. The transport of thermal energy in carbon nanotubes occurs through phonon conduction mechanism, similar to other non-metals. However, with the addition of 0.5 wt.% of MWCNTs, the thermal conductivity value decreases compared to MWCNTs-0.25. This decrease can be attributed to

the formation of MWCNT aggregates in the polymer matrix, which disrupt the thermal conduction pathways. These aggregates are formed due to strong Van der Waals forces between MWCNTs and are observed in the form of ropes or bundles. Hwang et al. observed a non-monotonic pattern concerning the MWCNT as filler concentration. The initial increase in thermal conductivity was ascribed to a uniform dispersion of fillers, while the subsequent decline was dominated by filler aggregation as the volumetric loading of MWCNT rises. When the matrix contains 1 wt.% MWCNT, the thermal conductivity decreases due to some MWCNTs have to bend or form agglomerates to fit into the limited packing volume [59]. A similar nonlinear trend in thermal conductivity with weight percent of MWCNT has been observed in by Im et al. and Patti et al. [60, 61].

The thermal conductivity of MWCNTs-1 is higher than that of MWCNTs-0.5 due to the formation of heat conduction pathways between the MWCNT aggregates [62]. A similar nonlinear trend in thermal conductivity with varying MWCNTs loading has been reported by Patti et al. The overall increase in thermal conductivity of MWCNTs ionogels compared to the base ionogel is attributed to the transport of a higher number of phonons occurring through MWCNTs, as compared to the amorphous polymer structure[63].

The thermal conductivity values of all ionogels range from 0.110 to 0.165 W/m·K, which are relatively low values, making the ionogels suitable candidates for thermoelectric materials. The maximum increase in thermal conductivity (11.3%) of ionogels with the temperature increase from 30 °C to 60 °C was observed for MWCNTs-0.25. This increase can be attributed to the decrease in the amount of MWCNT aggregates and an increase in the number of thermal conduction pathways in the polymer matrix.

3.8 Power factor and Thermoelectric Figure of Merit of Ionogels

According to Equation (4), the power factor (P) of a thermoelectric material can be calculated as the product of the square of the electrical conductivity (σ) and the Seebeck coefficient (S).

$$P = \sigma S^2 \quad (4)$$

Among the MWCNTs ionogels, the highest power factor of 4.19 $\mu W \cdot m^{-1} \cdot K^{-1}$ was observed for MWCNTs-0.25, as shown in Figure 9(a). When the electrical conductivity of a thermoelectric material increases due to an increase in the number of charge carriers, the Seebeck coefficient tends to decrease. In the case of MWCNTs-0.25 ionogels, the maximum Seebeck coefficient of 1.70 mV/K was observed, which corresponds to the minimum ionic conductivity among the MWCNTs ionogels.

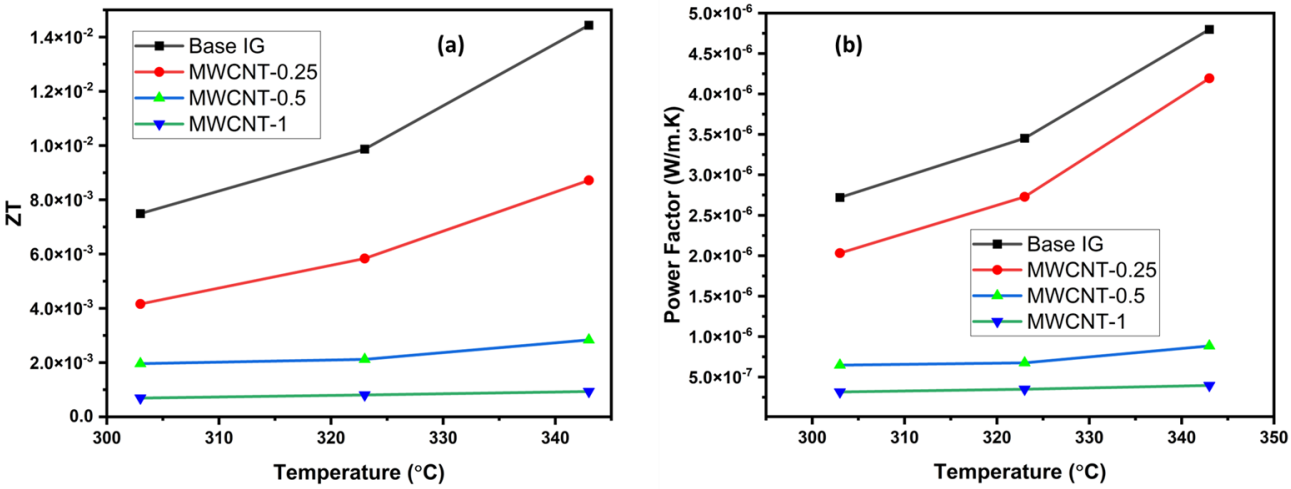

Fig. 9. (a) A plot of thermoelectric figure of merit (ZT) of ionogels versus temperature (b) A comparison of power factors of ionogels.

In Figure 9(b), the thermoelectric figure of merit (ZT) for the ionogels is plotted against temperature. It can be observed that all the ionogels showed a linear increase in ZT with increasing temperature. Among the different weight percentages of MWCNTs, the highest figure of merit ($ZT = 9 \times 10^{-3}$) was exhibited by MWCNTs-0.25. The synthesized novel

ionogels offer several advantages, including being eco-friendly and cost-effective, while simultaneously providing a higher Seebeck coefficient compared to electronic thermoelectric materials. This high Seebeck coefficient (1.93 mV/K for base IG and 1.70 mV/K for MWCNTs-0.25 IG) suggests potential applications in various areas such as ionic thermoelectric capacitors, electrochromic membrane bipolar diodes, and bipolar junction transistors.

3.9 Conclusions

In conclusion, this study demonstrates the successful synthesis of cross-linked thermoelectric ionogels through the thermal polymerization of polyethylene glycol dimethacrylate monomer with the inclusion of an ionic liquid and a free radical initiator. MWCNTs were incorporated into the base ionogel at three different concentrations: 0.25 wt. %, 0.5 wt. %, and 1 wt. %. The ionogels exhibited high thermoelectric performance, with the MWCNT-0.25 wt. % ionogel showing the highest Seebeck coefficient among the MWCNT ionogels. Furthermore, the MWCNT-0.25 wt. % ionogel demonstrated excellent thermal stability up to 386 °C. These findings can contribute to the development of novel thermoelectric materials based on ionogels.

Acknowledgment: R. Saidur and Mohd Faiz Mohd Salleh sincerely thankful for the financial support of the Sunway University through the project no# STR-RCTR-RCNMET-001-2019 and Universiti Malaya through grant number: FP062-2016 respectively. The authors also extend their appreciation to the Deanship of Scientific Research at King Khalid University for funding this work through the large group Research Project under grant number RGP.2 /303/44.

Conflicts of Interests: The authors declare that they have no known competing financial interests or personal relationships that could have appeared to influence the work reported in this paper.

Author Contributions:

Imran Haider Sajid: Investigation, Writing - original draft. Navid Aslfattahi: Data curation. Mohd Faizul Mohd Sabri: Supervision, review, and editing. Mohd Faiz Mohd Salleh: Visualization, Funding acquisition. Nik Nazri Nik Ghazali: Supervision, review, and editing. R.Saidur: Review, editing and Funding acquisition. Muhammad Tahir: Writing, review, and editing. Mohamed Bashir Ali Bashir: Writing, review, and editing.

References:

1. Gingerich, D.B. and M.S. Mauter, *Quantity, quality, and availability of waste heat from United States thermal power generation.* Environmental science +ACY- technology, 2015. **49**(14): p. 8297-8306.
2. Jagadish, P.R., *et al., Cost effective thermoelectric composites from recycled carbon fibre: From waste to energy.* Journal of Cleaner Production, 2018. **195**: p. 1015-1025.
3. Rahbar, K., *et al., Review of organic Rankine cycle for small-scale applications.* Energy conversion and management, 2017. **134**: p. 135-155.
4. Lee, S.W., *et al., An electrochemical system for efficiently harvesting low-grade heat energy.* Nature communications, 2014. **5**.
5. Bharti, M., *et al., Free-standing flexible multiwalled carbon nanotubes paper for wearable thermoelectric power generator.* Journal of Power Sources, 2019. **2274**.
6. Li, P., *et al., Facile green strategy for improving thermoelectric performance of carbon nanotube/polyaniline composites by ethanol treatment.* Composites Science and Technology, 2020. **189**.
7. Hasan, S.W., et al., *Optimization of poly(vinylidene fluoride) membranes for enhanced power density of thermally driven electrochemical cells.* Journal of Materials Science, 2017. **52**(17).
8. Song, H., *et al., Polymer/carbon nanotube composite materials for flexible thermoelectric power generator.* Composites Science and Technology, 2017. **153**: p. 71-83.
9. Liang, L., *et al., Ternary thermoelectric composites of polypyrrole/PEDOT: PSS/carbon nanotube with unique layered structure prepared by one-dimensional polymer nanostructure as template.* Composites Science and Technology, 2020. **187**.
10. Dörling, B., et al., *Exploring different doping mechanisms in thermoelectric polymer/carbon nanotube composites.* Synthetic Metals, 2017. **225**: p. 70-75.
11. Tee, B.C. and J. Ouyang, *Soft electronically functional polymeric composite materials for a flexible and stretchable digital future.* Advanced Materials, 2018. **30**(47): p. 1802560.
12. Yang, P., *et al., Wearable thermocells based on gel electrolytes for the utilization of body heat.* Angewandte Chemie International Edition, 2016. **55**(39): p. 12050-12053.
13. Mart+Ao0-n-Gonz+Aoe-lez, M., O. Caballero-Calero, and P. D+Ao0-az-Chao, *Nanoengineering thermoelectrics for 21st century: Energy harvesting and other trends in the field.* Renewable and Sustainable Energy Reviews, 2013. **24**: p. 288-305.
14. Dupont, M., D. MacFarlane, and J. Pringle, *Thermo-electrochemical cells for waste heat harvesting–progress and perspectives.* Chemical communications, 2017. **53**(47): p. 6288-6302.
15. Bulusu, A. and D. Walker, *Review of electronic transport models for thermoelectric materials.* Superlattices and Microstructures, 2008. **44**(1): p. 1-36.

16. Caballero-Calero, O., *et al., Improvement of Seebeck coefficient in as-grown Bi2Te3-ySey electrodeposited films by the addition of additives and bath optimization.* Electrochimica Acta, 2018. **269**: p. 490-498.
17. Danine, A., *et al., Microstructure and thermoelectric properties of p-type bismuth antimony telluride nanowires synthetized by template electrodeposition in polycarbonate membranes.* Electrochimica Acta, 2018. **279**: p. 258-268.
18. Perez-Taborda, J.A., et al., *High Thermoelectric zT in n-Type Silver Selenide films at Room Temperature.* Advanced Energy Materials, 2018. **8**(8): p. 1702024.
19. Ye, G., *et al., One-step electrodeposition of free-standing flexible conducting PEDOT derivative film and its electrochemical capacitive and thermoelectric performance.* Electrochimica Acta, 2017. **224**: p. 125-132.
20. Migita, T., *et al., Thermoelectromotive force of some redox couples in an amide-type room-temperature ionic liquid.* Electrochemistry, 2009. **77**(8): p. 639-641.
21. Duan, J., et al., *Aqueous thermogalvanic cells with a high Seebeck coefficient for low-grade heat harvest.* Nature communications, 2018. **9**(1): p. 5146.
22. De Anastro, A.F., *et al., Poly (ionic liquid) iongels for all-solid rechargeable zinc/PEDOT batteries.* Electrochimica Acta, 2018. **278**: p. 271-278.
23. Sajid, I.H., et al., *Crosslinked thermoelectric hydro-ionogels: A new class of highly conductive thermoelectric materials.* Energy Conversion and Management, 2019. **198**.
24. Du, Y., *et al., Preparation and thermoelectric properties of flexible SWCNT/PEDOT: PSS composite film.* Synthetic Metals, 2020. **261**.
25. Aghelinejad, M., Y. Zhang, and S.N. Leung, *Processing parameters to enhance the electrical conductivity and thermoelectric power factor of polypyrrole/multi-walled carbon nanotubes nanocomposites.* Synthetic Metals, 2019. **247**: p. 59-66.
26. Wang, L., *et al., Preparation and thermoelectric properties of polythiophene/multiwalled carbon nanotube composites.* Synthetic metals, 2013. **181**: p. 79-85.
27. Kim, S., *et al., Thermoelectric behavior of bulk-type functionalized-SWCNT incorporated Te nanowire/PMMA hybrid nanocomposites with a segregated structure.* Synthetic Metals, 2019. **254**: p. 56-62.
28. Song, H., *et al., Influence of polymerization method on the thermoelectric properties of multi-walled carbon nanotubes/polypyrrole composites.* Synthetic Metals, 2016. **211**: p. 58-65.
29. Fan, W., *et al., Toward high thermoelectric performance for polypyrrole composites by dynamic 3-phase interfacial electropolymerization and chemical doping of carbon nanotubes.* Composites Science and Technology, 2019. **183**.
30. Gnanaseelan, M., *et al., Cellulose-carbon nanotube composite aerogels as novel thermoelectric materials.* Composites Science and Technology, 2018. **163**: p. 133-140.
31. Qu, S., et al., *A novel hydrophilic pyridinium salt polymer/SWCNTs composite film for high thermoelectric performance.* Polymer, 2018. **136**: p. 149-156.
32. Duc, N.D., *et al., Thermal and mechanical stability of functionally graded carbon nanotubes (FG CNT)-reinforced composite truncated conical shells surrounded by the elastic foundations.* Thin-Walled Structures, 2017. **115**: p. 300-310.
33. Gong, T., *et al., Selective distribution and migration of carbon nanotubes enhanced electrical and mechanical performances in polyolefin elastomers.* Polymer, 2017. **110**: p. 1-11.
34. Kataoka, T., et al., *Highly conductive ionic-liquid gels prepared with orthogonal double networks of a low-molecular-weight gelator and cross-linked polymer.* ACS applied materials & interfaces, 2015. **7**(41): p. 23346-23352.
35. Sajid, I.H., et al., *Synthesis and characterization of novel p-type chemically cross-linked ionogels with high ionic seebeck coefficient for low-grade heat harvesting.* Electrochimica Acta, 2019. **320**.

36. Wang, Q., et al., *Room-temperature ionic liquids/multi-walled carbon nanotubes/chitosan composite electrode for electrochemical analysis of NADH.* Electrochimica acta, 2007. **52**(24): p. 6630-6637.
37. Jiao, X., et al., *Synthesis and studies of poly (ethylene glycol dimethacrylate) microcapsule.* Colloid and Polymer Science, 2016. **294**: p. 639-646.
38. Zhao, D., *et al., Polymerization mechanism of poly(ethylene glycol dimethacrylate) fragrance nanocapsules.* Rsc Advances, 2015. **5**(116): p. 96067-96073.
39. Łyszczek, R., et al., *Hybrid materials based on PEGDMA matrix and europium (III) carboxylates-thermal and luminescent investigations.* European Polymer Journal, 2018. **106**: p. 318-328.
40. Park, M.J., *et al., Covalent modification of multiwalled carbon nanotubes with imidazolium-based ionic liquids: effect of anions on solubility.* Chemistry of materials, 2006. **18**(6): p. 1546-1551.
41. Nava, D., et al., *An experimental and theoretical correlation to account for the effect of LiPF6 concentration on the ionic conductivity of poly (poly (ethylene glycol) methacrylate).* Solid State Ionics, 2016. **290**: p. 98-107.
42. Kim, D., P.K. Kannan, and C.H. Chung, *High-Performance Flexible Supercapacitors Based on Ionogel Electrolyte with an Enhanced Ionic Conductivity.* ChemistrySelect, 2018. **3**(7): p. 2190-2195.
43. Chen, L., et al., *Cross-linked polymeric ionic liquids ion gel electrolytes by in situ radical polymerization.* Chemical Engineering Journal, 2019. **378**: p. 122245.
44. Ngoma, M.M., M. Mathaba, and K. Moothi, *Effect of carbon nanotubes loading and pressure on the performance of a polyethersulfone (PES)/carbon nanotubes (CNT) membrane.* Scientific reports, 2021. **11**(1): p. 23805.
45. Moganty, S.S., *et al.* Ionic liquid-tethered nanoparticle suspensions: a novel class of ionogels, 2012. **24**(7): p. 1386-1392.
46. Fredlake, C.P., *et al.* Thermophysical properties of imidazolium-based ionic liquids, 2004. **49**(4): p. 954-964.
47. Yao, F., *et al.* Thermal decomposition kinetics of natural fibers: activation energy with dynamic thermogravimetric analysis, 2008. **93**(1): p. 90-98.
48. Zhou, T., et al., *Thermal properties and thermal stability of PP/MWCNT composites.* Composites Part B: Engineering, 2016. **90**: p. 107-114.
49. Wang, M., J. Hu, and M.D. Dickey, *Tough Ionogels: Synthesis, Toughening Mechanisms, and Mechanical Properties– A Perspective.* JACS Au, 2022. **2**(12): p. 2645-2657.
50. Susan, M.A., *et al., Ion gels prepared by in situ radical polymerization of vinyl monomers in an ionic liquid and their characterization as polymer electrolytes.* Journal of the American Chemical Society, 2005. **127**(13): p. 4976-4983.
51. Datta, R.S., *et al., Ionic liquid entrapment by an electrospun polymer nanofiber matrix as a high conductivity polymer electrolyte.* Rsc Advances, 2015. **5**(60): p. 48217-48223.
52. Shalu, et al., *Thermal stability, complexing behavior, and ionic transport of polymeric gel membranes based on polymer PVdF-HFP and ionic liquid,[BMIM][BF4].* The Journal of Physical Chemistry B, 2013. **117**(3): p. 897-906.
53. Petsagkourakis, I., *et al., Correlating the Seebeck coefficient of thermoelectric polymer thin films to their charge transport mechanism.* Organic Electronics, 2018. **52**: p. 335-341.
54. Pai, Y.H., et al., *Ionic Organic Thermoelectrics with Impressively High Thermopower for Sensitive Heat Harvesting Scenarios.* Advanced Energy Materials, 2023. **13**(1): p. 2202507.
55. Liu, S., et al., *Giant and bidirectionally tunable thermopower in nonaqueous ionogels enabled by selective ion doping.* Science advances, 2022. **8**(1): p. eabj3019.
56. Zhao, D., et al., *Polymer gels with tunable ionic Seebeck coefficient for ultra-sensitive printed thermopiles.* Nature communications, 2019. **10**(1): p. 1093.
57. Cheng, H., et al., *Flexible quasi-solid state ionogels with remarkable seebeck coefficient and high thermoelectric properties.* Advanced Energy Materials, 2019. **9**(32): p. 1901085.

58. Huang, C., X. Qian, and R. Yang, *Thermal conductivity of polymers and polymer nanocomposites.* Materials Science and Engineering: R: Reports, 2018. **132**: p. 1-22.
59. Hwang, Y., M. Kim, and J. Kim, *Improvement of the mechanical properties and thermal conductivity of poly (ether-ether-ketone) with the addition of graphene oxide-carbon nanotube hybrid fillers.* Composites Part A: Applied Science and Manufacturing, 2013. **55**: p. 195-202.
60. Im, H., et al., *The thermal conductivity of Al (OH) 3 covered MWCNT/epoxy terminated dimethyl polysiloxane composite based on analytical Al (OH) 3 covered MWCNT.* Composites Part A: Applied Science and Manufacturing, 2013. **54**: p. 159-165.
61. Patti, A., et al., *The effect of filler functionalization on dispersion and thermal conductivity of polypropylene/multi wall carbon nanotubes composites.* Composites Part B: Engineering, 2016. **94**: p. 350-359.
62. Das, A., et al., *Modified and unmodified multiwalled carbon nanotubes in high performance solution-styrene–butadiene and butadiene rubber blends.* Polymer, 2008. **49**(24): p. 5276-5283.
63. Gojny, F.H., *et al., Evaluation and identification of electrical and thermal conduction mechanisms in carbon nanotube/epoxy composites.* Polymer, 2006. **47**(6): p. 2036-2045.